Information-Theoretical Approach to Integrated Pulse-Doppler Radar and Communication Systems

Geon Choi
Dept. of EE, Korea University
Seoul, South Korea
geon.choi96@gmail.com

Namyoon Lee
Dept. of EE, Korea University
Seoul, South Korea
namyoon@korea.ac.kr

***Abstract*—Integrated sensing and communication improves the design of systems by combining sensing and communication functions for increased efficiency, accuracy, and cost savings. The optimal integration requires understanding the trade-off between sensing and communication, but this can be difficult due to the lack of unified performance metrics. In this paper, an information-theoretical approach is used to design the system with a unified metric. A sensing rate is introduced to measure the amount of information obtained by a pulse-Doppler radar system. We derive an lower bound of the sensing rate and establish it in terms of Neyman-Pearson detector. The simulation results explains the meaning of the sensing rate and trade-offs of sensing and communication systems.**

I. Introduction

The persistent trend of spectrum scarcity in wireless communications has prompted the development of Integrated Sensing and Communication (ISAC), a revolutionary approach to provide high-speed communication and precise sensing services within limited spectrum availability. Unlike traditional communication and sensing systems, which are independently designed with separate hardware platforms and orthogonal spectrums, ISAC optimizes the system by sharing bandwidth and hardware [1]–[5]. This joint design approach enhances spectral efficiency and sensing accuracy, while also reducing hardware costs. ISAC has gained popularity as a solution for emerging applications, including autonomous driving in vehicular networks, indoor positioning with WiFi signals, and joint radar imaging and communication systems [6]–[11].

The integration of sensing and communication systems presents a major challenge due to the lack of understanding of the trade-off between their performance when sharing the same radio spectrum. While the classical Shannon theory [12] outlines the limit of communication systems, it remains unclear what the maximum amount of reliable information can be obtained from unknown objects (e.g., distances, velocities, angle of arrivals, and reflected power levels) in a sensing system for a given time-frequency resource. Historically, radar systems have been designed to accurately estimate the features of unknown objects, with mean-squared error (MSE) [13] and Cramer-Rao lower bound (CRLB) [14] being popular performance metrics. However, the lack of a connection between Fisher information and mutual information in information theory impedes the design of integrated sensing and communication systems with a unified performance metric. Thus, a unified performance metric is crucial for optimal integration of these heterogeneous systems.

Significant progress has been made in recent years in characterizing a fundamental trade-off of ISAC systems within a unified framework. The pioneering work in [15]–[17] defines the radar estimation rate as the minimum required bits to encode the Kalman residual of target parameters such as range and velocity in a target tracking scenario. Using this notion, a trade-off between sensing and communication rates was characterized in different resource sharing scenarios. An information theoretic approach for an ISAC problem has also been introduced in [18]–[21]. The works in [18]–[20] consider a state-dependent stationary memoryless channel where the transmitter sends a message to a receiver and estimates the state of the channel using a strictly causal channel output feedback. In their setup, the trade-off of the ISAC system was studied under the rate-distortion theoretic framework. The work [21] considers the simultaneous binary state detection and data communication problem and characterizes a trade-off in terms of communication rate against the error exponent in detecting the binary channel state. Although these prior works have opened a new direction toward optimally integrating the sensing and communication systems from an information-theoretical viewpoint, these approaches still have limitations to understanding the sensing rate for widely-used pulse-Doppler radar systems in terms of practical system parameters such as signal bandwidth, target parameter resolution, and target statistics.

How much information rate is acquired by the pulse-Doppler radar system from targets in an environment? In this paper, we address this question by introducing a new concept - the sensing rate of a range-Doppler radar system. This rate is calculated as a combination of range, Doppler resolutions, and target's statistical distributions. Unlike previous works in [15]–[17], [22]–[24] that utilize CRLB, our approach is based on more practical models and assumptions of the pulse-Doppler radar system. The key contributions of this paper are outlined below:

- We introduce the concept of sensing rate, which quantifies the amount of information obtained from a target in terms of bits per channel use. By utilizing the I-MMSE relationship from [25], we derive an exact expression for the sensing rate in integral form.

ISBN 978-3-903176-65-2 © 2024 IFIP

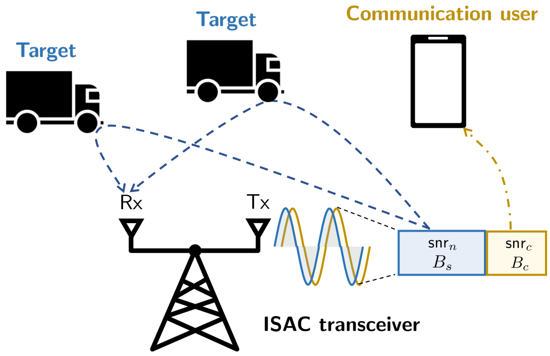

Fig. 1. An illustration of a ISAC system model.

- We also derive a tight lower bound of the sensing rate. This expression is valuable in comprehending how the sensing rate varies based on system parameters. The derived lower bound of the sensing rate clearly indicates that the rate is directly proportional to the target uncertainty in the range-Doppler plane and the target signal-to-noise ratio (SNR). This expression establishes a connection between information-theoretic measures and estimation-theoretic measures, such as the minimum target detection error probability and the minimum MSE of target RCS. Our simulations validate the accuracy of the derived expression.
- We numerically study trade-offs of sensing and communication systems. Simulation results show that the additional sensing bandwidth yields additional sensing information, while additional power serves additional sensing information only when the sensing system is in power-hungry state.

II. System Model

In this section, we present an ISAC system model. As illustrated in Fig. 1, an ISAC transceiver sends a pulse train and receives echoes for sensing an unknown environment. Meanwhile, it also transmits a message to a receiver for communications. The total system bandwidth is assumed to be B, and the sensing and communication systems use a fraction of the total bandwidth, i.e., $B_\mathrm{s} = \lambda B$ and $B_\mathrm{c} = (1-\lambda)B$ for $\lambda \in [0, 1]$. We explain the signal models for the sensing system, and then define the performance metric for the ISAC system.

A. Pulse-Doppler Radar and Range-Doppler Map

The radar sends signal $x(t)$ comprised of M narrowband pulses $g(t)$ with pulse repetition interval (PRI) T_p during coherent processing interval (CPI) as

$$x(t) = \sum_{m=0}^{M-1} g(t - mT_\mathrm{p}), \qquad 0 \le t \le MT_\mathrm{p}, \tag{1}$$

where the pulse $g(t)$ has the bandwidth of $B_\mathrm{s} = 1/T_\mathrm{s}$ and transmit energy $\int_0^{T_\mathrm{s}} |g(t)|^2 \mathrm{d}t = P_\mathrm{t} T_\mathrm{s}$. This transmitted signal is reflected by targets in an unknown environment.

We adopt the Swerling I target model [26]. This target model has been widely used to capture a static environmental scenario in the time scale of CPI. In this model, L non-fluctuating point targets are well-spread during CPI, and L targets are assumed to be statistically independent. Each target is defined by three parameters: i) range d_ℓ, ii) radial velocity v_ℓ, and iii) complex amplitude H_ℓ for $\ell \in [L]$. The range and the radial velocity of target ℓ correspond to round-trip time-delay $\tau_\ell = 2d_\ell/c$ and normalized doppler frequency $\nu_\ell = 2f_c v_\ell/c$. The complex amplitude H_ℓ is assumed to be drawn from IID complex Gaussian with mean $\mu_{T,\ell}$ and variance $\sigma_{T,\ell}^2$, i.e., $H_\ell \sim \mathcal{CN}(\mu_{T,\ell}, \sigma_{T,\ell}^2)$ for $\ell \in [L]$.

In addition, we assume that the radar system operates under the following target assumptions:

- The target parameters $\{\tau_\ell, \nu_\ell, H_\ell\}_{\ell=1}^L$ are constant during CPI. This implies that the target state changes slowly.
- Target range and velocity are limited such that the following conditions i) $\tau_\ell/T_\mathrm{s} = U_\ell$ for $U_\ell \in \{0, \dots, N-1\}$ and $N = \lfloor T_\mathrm{p}/T_\mathrm{s} \rfloor$, ii) $\nu_\ell T_\mathrm{p} = V_\ell/M$ for $V_\ell \in \{0, \dots, M-1\}$, and iii) $(\tau_\ell, \nu_\ell) \neq (\tau_{\ell'}, \nu_{\ell'})$ for $\ell \neq \ell'$ are satisfied. That is, every target is on the Nyquist sampling grid after sampling with rate $1/T_\mathrm{s}$, and separable.

The continuous-time baseband received signal from the target reflections during CPI is given by

$$y(t) = \sum_{m=0}^{M-1} \sum_{\ell=1}^{L} \sqrt{\beta_\ell} H_\ell g(t - \tau_\ell - mT_\mathrm{p}) e^{j2\pi m \nu_\ell t} + w(t), \tag{2}$$

where $w(t)$ is the complex additive white Gaussian noise with mean zero and variance $B_\mathrm{s} N_0$, which is defined as the product of signal bandwidth B_s and noise spectral density N_0. In addition, β_ℓ is the received signal power from the ℓth target reflection, which is defined by the classical radar equation:

$$\beta_\ell = \frac{P_\mathrm{t} G_\mathrm{t}}{4\pi d_\ell^2} \frac{\sigma_\mathrm{rcs} A_\mathrm{eff}}{4\pi d_\ell^2}, \tag{3}$$

where σ_rcs denotes the RCS of a target measured in m^2, and A_eff is the effective area of the receiving antenna.

The classical pulse-Doppler radar system performs two sequential post-processing: i) fast-time and ii) slow-time processing on (2) to estimate target parameters $\{\tau_\ell, \nu_\ell, H_\ell\}_{\ell=1}^L$. After post-processing, the received samples constitute range-Doppler map, which is modeled by

$$Y_{n,k} = \sqrt{\mathsf{snr}_n} X_{n,k} + Z_{n,k}, \tag{4}$$

where $Z_{n,k}$ is the normalized noise, which follows the complex Gaussian with zero-mean and unit variance, i.e., $Z_{n,k} \sim \mathcal{CN}(0, 1)$, and $X_{n,k}$ is the target signal, given by

$$X_{n,k} = \sum_{\ell=1}^{L} H_\ell \delta[n - U_\ell] \delta[k - V_\ell]. \tag{5}$$

The derivation of (5) is further illustrated in Appendix I.

From (5), we model that target returned signal $X_{n,k}$ is distributed as a Bernoulli-Gaussian (BG) random variable, i.e.,

$$f_{X_{n,k}}(x_{n,k}) = (1-\gamma)\delta(x_{n,k}) + \gamma \frac{1}{\pi\sigma_{\mathsf{T}}^2} e^{-\frac{(x_{n,k}-\mu_{\mathsf{T}})^2}{\sigma_{\mathsf{T}}^2}}, \quad (6)$$

where $\gamma \in (0,1)$ determines the probability that $X_{n,k}$ is a non-zero value. We shall use a short notation $X_{n,k} \sim \mathsf{BG}(x|\mu_{\mathsf{T}}, \sigma_{\mathsf{T}}^2, \gamma)$ in the sequel.

Remark 1: The parameter γ determines the sparsity level of $X_{n,k}$ in the range-Doppler plane. This parameter γ contains a prior knowledge about environment. For instance, if the system is blind to the environment, one can choose $\gamma = 1/2$. However, when L targets on average have been detected in the previous CPIs, one can choose $\gamma = \frac{L}{MN}$. In this work, we focus on the specific CPI and assume γ to be a pre-determined parameter.

B. Performance Metrics

We shall characterize the *sensing spectral efficiency* of the pulse-Doppler radar system. An information theoretical approach to measure the information rate between $X_{n,k}$ and $Y_{n,k}$ is given by

$$R_{n,k}(\mathsf{snr}_n) = I(X_{n,k}; Y_{n,k}) \quad \text{(bits/sec/Hz)}, \quad (7)$$

for $n \in \{0, 1, \ldots, N-1\}$ and $k \in \{0, 1, \ldots, M-1\}$. It is noteworthy that the number of range bins N depends on the sensing bandwidth according to the Rayleigh criterion, which states that the range resolution is the inverse of the signal bandwidth [13]. This mutual information measures the amount of information acquired from the environment placed at the (n,k) range-Doppler bin. Since the mutual information differs across the range bins only, we define the average sensing rate as

$$R_{\mathrm{s}}(B_{\mathrm{s}}, \mathsf{snr}_n) = \frac{B_{\mathrm{s}}}{NM} \sum_{n=0}^{N-1} \sum_{k=0}^{M-1} R_{n,k}(\mathsf{snr}_n) \quad \text{(bits/sec)}. \quad (8)$$

This average information rate is the amount of information attained by sensing the target environment per second.

For the communication system, we consider the Gaussian channel. In the Gaussian channel, the communication rate with bandwidth B_{c} is given by

$$R_{\mathrm{c}}(B_{\mathrm{c}}, \mathsf{snr}_{\mathsf{c}}) = B_{\mathrm{c}} \log_2(1 + \mathsf{snr}_c) \quad \text{(bits/sec)}, \quad (9)$$

where $\mathsf{snr}_{\mathrm{c}}$ is the received SNR of communication system. Intuitively, increasing power and bandwidth for the range-Doppler radar system can improve sensing rate R_{s} while decreasing communication rate R_{c}. As a result, it is crucial to understand a trade-off between the sensing and communication rates according to the system resources. To measure this trade-off, we define a weighted sum spectral efficiency as

$$R_{\mathrm{sum}} = \frac{w_{\mathrm{s}} R_{\mathrm{s}}(B_{\mathrm{s}}, \mathsf{snr}_n) + w_{\mathrm{c}} R_{\mathrm{c}}(B_{\mathrm{c}}, \mathsf{snr}_c)}{B_{\mathrm{s}} + B_{\mathrm{c}}} \quad \text{(bits/sec/Hz)}, \quad (10)$$

where w_{s} and w_{c} are weights for sensing and communication rates, respectively.

Remark 2: The system weights w_{s} and w_{c} can be chosen according to priority aspects of sensing and communication functions. For instance, the communication system for emergency broadcasting system is assigned higher weight than system for usual data transmission. The intrinsic disparity of two system can be incorporated into those weights [17]. The sensing system requires more power to obtain 1 bit than communication system because sensing system is regarded as uncooperative communication system. The high power demanding system weight can be assigned to be higher than other systems.

III. Sensing Rate Characterization

In this section, we express the sensing rate in terms of estimation-theoretic quantity by applying the I-MMSE relationship in [25]. In addition, we provide the lower bound of the sensing rate, which is expressed in terms of quantities of detection theory.

A. An Exact Expression

The I-MMSE relationship is a foundation that provides a deep connection between an information- and an estimation-theoretic quantity [25]. The I-MMSE relationship states that the integration of MMSE is the mutual information for an arbitrary target distribution $f_{X_{n,k}}(x_{n,k})$ with a finite moment $\mathbb{E}\left[X_{n,k}^2\right] < \infty$ [25]. As a stepping stone, we provide the MMSE estimator and the resultant MMSE.

Lemma 1: The MMSE estimator for the target signal in the (n,k) range-Doppler bin is given by

$$\begin{aligned} &\hat{X}_{n,k}^{\mathsf{mmse}}(y_{n,k}; \mathsf{snr}_n) \\ &= \mathbb{E}[X_{n,k} | Y_{n,k} = y_{n,k}; \mathsf{snr}_n] \\ &= \frac{\mu_{\mathsf{T}} + \frac{\sqrt{\mathsf{snr}_n}\sigma_{\mathsf{T}}}{1+\mathsf{snr}_n\sigma_{\mathsf{T}}^2}\left(y_{n,k} - \sqrt{\mathsf{snr}_n}\mu_{\mathsf{T}}\right)}{1 + \frac{1-\gamma}{\gamma}(\mathsf{snr}_n\sigma_{\mathsf{T}}^2 + 1)e^{-|y_{n,k}|^2 + \frac{|y_{n,k} - \sqrt{\mathsf{snr}_n}\mu_{\mathsf{T}}|^2}{\mathsf{snr}_n\sigma_{\mathsf{T}}^2+1}}}. \end{aligned} \quad (11)$$

The resultant MMSE is given by

$$\mathsf{mmse}_{n,k}(\mathsf{snr}_n) = \mathbb{E}\left[\left(X_{n,k} - \hat{X}_{n,k}^{\mathsf{mmse}}(Y_{n,k})\right)^2; \mathsf{snr}_n\right] \quad (12)$$

Proof: See Appendix II-A. ∎

Using the derived MMSE expression, the sensing rate is given by the following Theorem.

Theorem 1: The sensing rate $R_{n,k}(\mathsf{snr}_n) = I(X_{n,k}; Y_{n,k})$ for (n,k) range-Doppler bin is given by

$$R_{n,k}(\mathsf{snr}_n) = \log_2 e \int_0^{\mathsf{snr}_n} \mathsf{mmse}_{n,k}(s)\mathrm{d}s. \quad (13)$$

Proof: The proof is the direct consequence of the I-MMSE relationship in [25]. ∎

From Theorem 1, it is evident that the information rate is an increasing function with snr_n by the non-negativity of $\mathsf{mmse}_{n,k}(s)$ for $s > 0$. Although the expression in (13) is exact and has full generality, this analytical expression of the sensing rate is intractable to understanding how the target parameters, $(\mu_{\mathsf{T}}, \sigma_{\mathsf{T}}, \gamma)$, change the information rate.

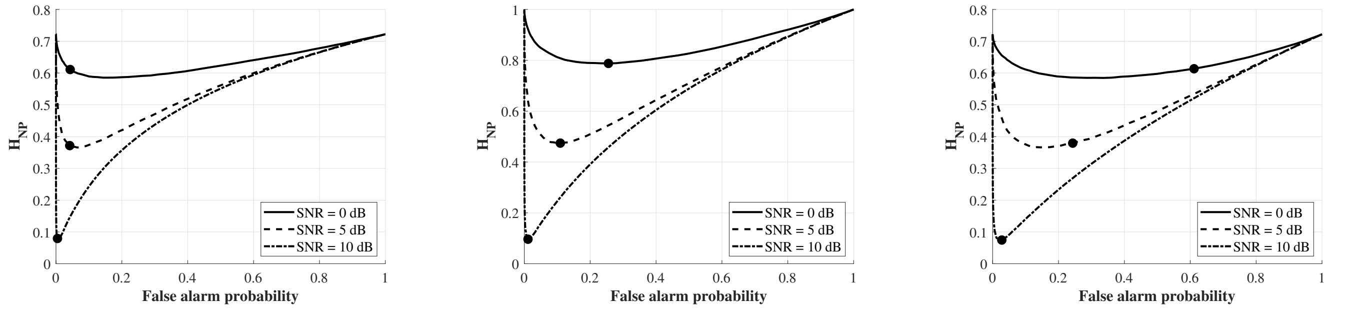

(a) $\gamma = 0.2$ (b) $\gamma = 0.5$ (c) $\gamma = 0.8$

Fig. 2. Remaining uncertainty $H_{\mathsf{NP}}(\gamma, P_{\mathsf{FA}}, P_{\mathsf{MD}})$ after detection and false alarm probability P_{FA} when applying NP detector. The circle marker is obtained by MAP detector. Target statistics: $\mu_{\mathsf{T}} = 1$, $\sigma_{\mathsf{T}}^2 = 0$, $\mathsf{snr}_n \in \{0, 5, 10\}$ [dB].

B. A Lower Bound

Before deriving into a lower bound of the sensing rate, which provide a connection to classical radar detectors, we briefly review Neyman-Pearson (NP) detector. Let us consider a binary target detector $g(\cdot) : \mathbb{C} \to \{0, 1\}$ which maps received signal $Y_{n,k}$ to a binary value according to the target presence. Armed with this binary detector, we define two types of probability errors as

$$\begin{aligned} P_{\mathsf{FA}}(\mathsf{snr}_n) &= \mathbb{P}[g(Y_{n,k}) = 1 \mid X_{n,k} = 0], \\ P_{\mathsf{MD}}(\mathsf{snr}_n) &= \mathbb{P}[g(Y_{n,k}) = 0 \mid X_{n,k} \neq 0], \end{aligned} \tag{14}$$

where P_{FA} is false alarm probability and P_{MD} is misdetection probability. Then, an average probability error is given by

$$P_{\mathsf{E}}(\gamma, \mathsf{snr}_n) = \gamma P_{\mathsf{MD}}(\mathsf{snr}_n) + (1 - \gamma) P_{\mathsf{FA}}(\mathsf{snr}_n). \tag{15}$$

The NP detector minimizes the misdetection probability among all detectors with false alarm probability no greater than threshold P_{FA}. According to the celebrated NP rule, the NP detector boils down to likelihood ratio testing given by

$$g_{\mathsf{NP}}(Y_{n,k}) = \begin{cases} 0, & \frac{\mathbb{P}(Y_{n,k} | X_{n,k} \neq 0)}{\mathbb{P}(Y_{n,k} | X_{n,k} = 0)} < \delta, \\ 1, & \frac{\mathbb{P}(Y_{n,k} | X_{n,k} \neq 0)}{\mathbb{P}(Y_{n,k} | X_{n,k} = 0)} > \delta. \end{cases} \tag{16}$$

Here, the threshold δ is determined by the maximum acceptable P_{FA}. As a note, it is worthwhile mentioning that a maximum a posterior detector is equivalent to the NP detector if the threshold parameter is chosen as $\delta = (1 - \gamma)/\gamma$.

To find the error probability expressions, we define the region as

$$\mathcal{A}(\mathsf{snr}_n) = \left\{ y_{n,k} \in \mathbb{C} \,\middle|\, \frac{\mathbb{P}(Y_{n,k} | X_{n,k} \neq 0)}{\mathbb{P}(Y_{n,k} | X_{n,k} = 0)} > \delta \right\}. \tag{17}$$

Then, the false alarm probability P_{FA} and misdetection probability P_{MD} when using the NP detector are given by

$$P_{\mathsf{FA}}(\mathsf{snr}_n) = \int_{y \in \mathcal{A}(\mathsf{snr}_n)} \frac{1}{\pi} e^{-|y|^2} \mathrm{d}y \tag{18}$$

and

$$P_{\mathsf{MD}}(\mathsf{snr}_n) = \int_{y \notin \mathcal{A}(\mathsf{snr}_n)} \frac{1}{\pi(\mathsf{snr}_n \sigma_{\mathsf{T}}^2 + 1)} e^{-\frac{|y - \sqrt{\mathsf{snr}_n} \mu_{\mathsf{T}}|^2}{\mathsf{snr}_n \sigma_{\mathsf{T}}^2 + 1}} \mathrm{d}y. \tag{19}$$

Now, we are ready to present a lower bound of the sensing rate.

Theorem 2: Let $\mathsf{H}_b(p) = -p \log p - (1 - p) \log(1 - p)$ be a binary entropy function with parameter $p \in [0, 1]$. Then, the sensing rate for the (n, k) range-Doppler bin $I(X_{n,k}; Y_{n,k})$ is lower bounded by

$$\begin{aligned} &I(X_{n,k}; Y_{n,k}) \\ &\quad \geq \mathsf{H}_b(\gamma) - \mathsf{H}_{\mathsf{NP}}(\gamma, P_{\mathsf{FA}}, P_{\mathsf{MD}}) + \gamma \log_2(1 + \mathsf{snr}_n \sigma_{\mathsf{T}}^2), \end{aligned} \tag{20}$$

where P_{FA} and P_{MD} is the false alarm and mis-detection error probability of (16) and

$$\begin{aligned} &\mathsf{H}_{\mathsf{NP}}(\gamma, P_{\mathsf{FA}}, P_{\mathsf{MD}}) \\ &\quad = \mathsf{H}_b(\gamma) + (1 - \gamma)\mathsf{H}_b(P_{\mathsf{FA}}) + \gamma \mathsf{H}_b(P_{\mathsf{MD}}) \\ &\qquad - \mathsf{H}_b((1 - \gamma) P_{\mathsf{FA}} + \gamma(1 - P_{\mathsf{MD}})). \end{aligned} \tag{21}$$

Proof: See Appendix II-B. ■

Theorem 2 elucidates how the sensing rate changes according to the target parameters and target detector. To be specific, the sensing rate can be decomposed into three parts. The first part $\mathsf{H}_b(\gamma)$ measures the uncertainty of the target localized at a specific (n, k) range-Doppler bin. In other words, this part provides the target's location and velocity information in a two-dimensional data matrix. This information rate increases when target presence probability γ is close to 1/2, which aligns with our intuition that more underlying uncertainty about target presence increases the sensing rate. This information rate, however, is reduced by the target detection error, $\mathsf{H}_{\mathsf{NP}}(\gamma, P_{\mathsf{FA}}, P_{\mathsf{MD}})$. As a result, the sensing rate can diminish as the error probability increases (e.g., low SNR or using sub-optimal detectors) as shown in Fig. 2. The last part $\gamma \log_2\left(1 + \mathsf{snr}_n \sigma_{\mathsf{T}}^2\right)$ measures the amount of information rate acquired from the target's returned signal under the target presence with probability γ. This rate is proportional to both the target's presence probability γ and the target signal variance σ_{T}^2 for given SNR.

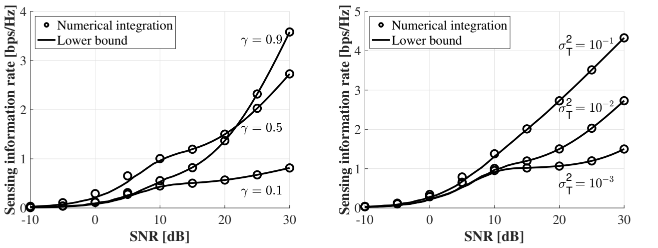

(a) (b)

Fig. 3. Illustration to verify the tightness of the lower bound in Theorem 2. Target signal statistics: (a) $\gamma \in \{0.1, 0.5, 0.9\}$, $\mu_{\mathsf{T}} = 1$, and $\sigma_{\mathsf{T}}^2 = 10^{-2}$, (b) $\gamma = 0.5$, $\mu_{\mathsf{T}} = 1$, and $\sigma_{\mathsf{T}}^2 \in \{10^{-1}, 10^{-2}, 10^{-3}\}$.

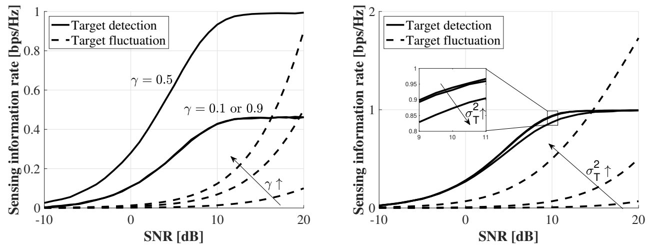

(a) (b)

Fig. 4. Illustration of decomposed sensing rate. Target signal statistics: (a) $\gamma \in \{0.1, 0.5, 0.9\}$, $\mu_{\mathsf{T}} = 1$, and $\sigma_{\mathsf{T}}^2 = 10^{-2}$, (b) $\gamma = 0.5$, $\mu_{\mathsf{T}} = 1$, and $\sigma_{\mathsf{T}}^2 \in \{10^{-1}, 10^{-2}, 10^{-3}\}$.

IV. Numerical results

This section presents the numerical simulation results of the sensing rate and its trade-off of sensing and communication systems.

A. Sensing Rate

We verify the Theorem 2. In addition, we decompose the sensing rate into two types of information to obtain a more detailed understanding.

Tightness of the lower bound: We provide numerical results to verify the exactness of the derived rate expression in Theorem 2. Fig. 3 shows that our lower bound expressions are very tight at all SNRs. The gap between exact rate and lower bound implies the loss of information after hard-decision.

The decomposed information: To shed light on the behavior of sensing rate, we provide numerical results of *target detection information* and *target fluctuation information* separately in Fig. 4. We define i) a binary random variable $U_{n,k} \in \{0, 1\}$ with Bernoulli parameter γ to denote the target presence at the (n, k) range-Doppler bin and ii) the target complex amplitude parameter $A_{n,k}$, which is drawn from $\mathcal{CN}(\mu_{\mathsf{T}}, \sigma_{\mathsf{T}}^2)$. Then, our BG target signal $X_{n,k} \sim \mathsf{BG}(x|\mu_{\mathsf{T}}, \sigma_{\mathsf{T}}^2, \gamma)$ can be represented in a vector form $(U_{n,k}, A_{n,k})$ and the sensing rate is decomposed as

$$I(X_{n,k}; Y_{n,k}) = I(U_{n,k}; Y_{n,k}) + \gamma \log_2\left(1 + \mathsf{snr}_n \sigma_{\mathsf{T}}^2\right). \quad (22)$$

Here, we name $I(U_{n,k}; Y_{n,k})$ as target detection information and $I(A_{n,k}; Y_{n,k}|U_{n,k} = 1)$ as target fluctuation information.

Fig. 4 shows the behavior of two types of information rate. The target detection information is dominant in the low SNR regime, and the target fluctuation information is dominant in the high SNR regime. It means that the target detection ability is important at low SNR. At the high SNR regime, the target signal estimation precision contributes to the sensing rate rather than target detection accuracy. Especially in Fig. 4-(b), the target detection information decreases as the target fluctuation σ_{T}^2 increases because the fluctuation hinders the target detection; thereby, more uncertainty is remained after the decision. The decomposed information explains the shape of curve in Fig. 3 as well.

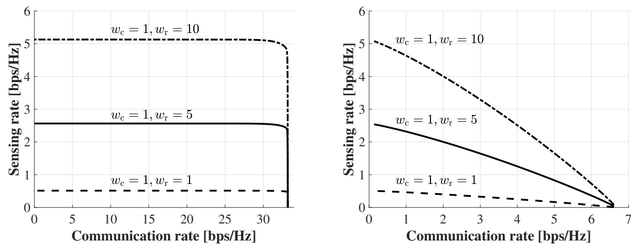

(a) Power trade-off (b) Bandwidth trade-off

Fig. 5. Trade-off of sensing and communication systems. Target signal statistics: $\gamma = 0.1$, $\mu_{\mathsf{T}} = 1$, and $\sigma_{\mathsf{T}}^2 = 10^{-2}$. (a) $B_c = B_s = 100$ MHz and $\mathsf{snr}_c + \max_n(\mathsf{snr}_n) = 100$ dB. (b) $\mathsf{snr}_c = 20$ dB, $\mathsf{snr}_c + \max_n(\mathsf{snr}_n) = 100$ dB, and $B_c + B_s = 200$ MHz.

B. Information Rate Trade-off

We use the Rayleigh criterion to determine the range resolution and sensing bandwidth. The maximum detection range is set to be 10 km. Fig. 5 presents the information rate trade-off of sensing and communication systems for various system weights. From the power trade-off, we can observe the threshold related to power efficiency. In contrast, the additional sensing bandwidth increases sensing rate. This result from the constant γ. Increasing the sensing bandwidth improves the resolution of range-Doppler map, and the increased resolution gives more chance to discover new targets in the environment.

V. Conclusion

By utilizing an information-theoretic approach, we evaluated the performance of the ISAC system by characterizing the amount of information that the pulse-Doppler radar can obtain. First, we defined the sensing rate of an unknown environment when using the pulse-Doppler radar and established connections with various radar system parameters and Neyman-Pearson detector. Then, by incorporating the sensing rate and Shannon's communication rate into the ISAC system, we numerically study trade-offs of sensing and communication systems. The major implication was that the trade-off rate of additional power and bandwidth to information rate is different. Simulation results also verified the exactness of the derived lower-bound expression.

References

[1] J. A. Zhang, F. Liu, C. Masouros, R. W. Heath, Z. Feng, L. Zheng, and A. Petropulu, "An overview of signal processing techniques for joint communication and radar sensing," *IEEE J. Sel. Topics Signal Process.*, vol. 15, no. 6, pp. 1295–1315, Nov. 2021.

[2] Y. Cui, F. Liu, X. Jing, and J. Mu, "Integrating sensing and communications for ubiquitous IoT: Applications, trends, and challenges," *IEEE Netw.*, vol. 35, no. 5, pp. 158–167, Sep. 2021.

[3] F. Liu, C. Masouros, A. P. Petropulu, H. Griffiths, and L. Hanzo, "Joint radar and communication design: Applications, state-of-the-art, and the road ahead," *IEEE Trans. Commun.*, vol. 68, no. 6, pp. 3834–3862, Jun. 2020.

[4] K. V. Mishra, M. B. Shankar, V. Koivunen, B. Ottersten, and S. A. Vorobyov, "Toward millimeter-wave joint radar communications: A signal processing perspective," *IEEE Signal Process. Mag.*, vol. 36, no. 5, pp. 100–114, Sep. 2019.

[5] L. Zheng, M. Lops, Y. C. Eldar, and X. Wang, "Radar and communication coexistence: An overview: A review of recent methods," *IEEE Signal Process. Mag.*, vol. 36, no. 5, pp. 85–99, Sep. 2019.

[6] D. Ma, N. Shlezinger, T. Huang, Y. Liu, and Y. C. Eldar, "Joint radar-communication strategies for autonomous vehicles: Combining two key automotive technologies," *IEEE Signal Process. Mag.*, vol. 37, no. 4, pp. 85–97, Jul. 2020.

[7] P. Kumari, D. H. N. Nguyen, and R. W. Heath, "Performance trade-off in an adaptive IEEE 802.11ad waveform design for a joint automotive radar and communication system," in *Proc. IEEE Int. Conf. Acoustic Speech Signal Processing (ICASSP)*, Mar. 2017, pp. 4281–4285.

[8] G. Wang, Y. Zou, Z. Zhou, K. Wu, and L. M. Ni, "We can hear you with Wi-Fi!" *IEEE Trans. Mobile Comput.*, vol. 15, no. 11, pp. 2907–2920, Nov. 2016.

[9] F. Colone, D. Pastina, P. Falcone, and P. Lombardo, "WiFi-based passive ISAR for high-resolution cross-range profiling of moving targets," *IEEE Trans. Geosci. Remote Sens.*, vol. 52, no. 6, pp. 3486–3501, Jun. 2014.

[10] R. Sankar, S. P. Chepuri, and Y. C. Eldar, "Beamforming in integrated sensing and communication systems with reconfigurable intelligent surfaces," *arXiv preprint arXiv:2206.07679*, 2022.

[11] X. Liu, T. Huang, Y. Liu, and Y. C. Eldar, "Transmit beamforming with fixed covariance for integrated MIMO radar and multiuser communications," in *Proc. IEEE Int. Conf. Acoustic Speech Signal Processing (ICASSP)*, May 2022, pp. 8732–8736.

[12] C. E. Shannon, "A mathematical theory of communication," *Bell System Technical Journal*, vol. 27, no. 3, pp. 379–423, Jul. 1948.

[13] M. A. Richards, J. Scheer, and W. A. Holm, *Principles of Modern Radar: Basic Principles*. New York, NY, USA: Scitech, 2010.

[14] H. V. Poor, *An Introduction to Signal Detection and Estimation*. New York: Springer-Verlag, 1994.

[15] A. R. Chiriyath, B. Paul, G. M. Jacyna, and D. W. Bliss, "Inner bounds on performance of radar and communications co-existence," *IEEE Trans. Signal Process.*, vol. 64, no. 2, pp. 464–474, Jan. 2016.

[16] B. Paul and D. W. Bliss, "Extending joint radar-communications bounds for FMCW radar with Doppler estimation," in *Proc. IEEE Radar Conf.*, May 2015, pp. 89–94.

[17] A. R. Chiriyath, B. Paul, and D. W. Bliss, "Radar-communications convergence: Coexistence, cooperation, and co-design," *IEEE Trans. Cogn. Commun. Netw.*, vol. 3, no. 1, pp. 1–12, Mar. 2017.

[18] M. Kobayashi, G. Caire, and G. Kramer, "Joint state sensing and communication: Optimal tradeoff for a memoryless case," in *Proc. IEEE Int. Symp. Inf. Theory (ISIT)*, Jun. 2018, pp. 111–115.

[19] M. Kobayashi, H. Hamad, G. Kramer, and G. Caire, "Joint state sensing and communication over memoryless multiple access channels," in *Proc. IEEE Int. Symp. Inf. Theory (ISIT)*, Jul. 2019, pp. 270–274.

[20] M. Ahmadipour, M. Wigger, and M. Kobayashi, "Joint sensing and communication over memoryless broadcast channels," in *Proc. IEEE Inf. Theory Workshop (ITW)*, Apr. 2021, pp. 1–5.

[21] H. Joudeh and F. M. Willems, "Joint communication and binary state detection," *IEEE J. Sel. Areas Inf. Theory*, vol. 3, no. 1, pp. 113–124, Mar. 2022.

[22] Q. He, Z. Wang, J. Hu, and R. S. Blum, "Performance gains from cooperative MIMO radar and MIMO communication systems," *IEEE Signal Process. Lett.*, vol. 26, no. 1, pp. 194–198, Nov. 2018.

[23] Y. Xiong, F. Liu, Y. Cui, W. Yuan, and T. X. Han, "Flowing the information from Shannon to Fisher: Towards the fundamental tradeoff in ISAC," *arXiv preprint arXiv:2204.06938*, 2022, [Online]. Available: https://arxiv.org/abs/2204.06938.

[24] F. Liu, Y.-F. Liu, A. Li, C. Masouros, and Y. C. Eldar, "Cramér-Rao bound optimization for joint radar-communication beamforming," *IEEE Trans. Signal Process.*, vol. 70, pp. 240–253, Dec. 2021.

[25] D. Guo, S. Shamai, and S. Verdú, "Mutual information and minimum mean-square error in Gaussian channels," *IEEE Trans. Inf. Theory*, vol. 51, no. 4, pp. 1261–1282, Apr. 2005.

[26] P. Swerling, "Probability of detection for fluctuating targets," *IRE Trans. Inf. Theory*, vol. 6, no. 2, pp. 269–308, Apr. 1960.

Appendix I
Rande-Doppler map model

Let $x_m(t)$ be the noise-free received signal during the mth PRI, which is defined as

$$x_m(t) = \sum_{\ell=1}^{L} \sqrt{\beta_\ell} H_\ell g(t - \tau_\ell - mT_\mathrm{p}) e^{-j2\pi m \nu_\ell T_\mathrm{p}} \qquad (23)$$

for $mT_\mathrm{p} \le t < (m+1)T_\mathrm{p}$. Using $x_m(t)$, we can rewrite the received signal in (2) during the mth PRI as

$$y_m(t) = x_m(t) + w_m(t), \qquad (24)$$

where $x_m(t)$ and $w_m(t)$ are the fraction of $x(t)$ and $w(t)$ for $mT_\mathrm{p} \le t < (m+1)T_\mathrm{p}$. The noise-free returned signal $x_m(t)$ can be interpreted as the transmitted signal by the environment, i.e., a target signal. As a result, from a communication system perspective, the target signal plays the role of the transmitted signal by the targets.

1) Radar post-processing: The main task of the pulse-Doppler radar is to identify $3L$ parameters $\{\tau_\ell, \nu_\ell, H_\ell\}_{\ell=1}^{L}$ from the received signal $y(t)$ during CPI as in (2) and (23). To this end, the classical pulse-Doppler radar system performs two sequential post-processing: i) fast-time and ii) slow-time processing. Applying the post-processing, we can obtain a discrete-time equivalent signal model.

Fast-time processing: The fast-time processing allows obtaining the discrete-time samples of the returned signal using matched filtering and sampling. After the matched filtering and sampling at the Nyquist rate $T_\mathrm{s} = 1/B_\mathrm{s}$, the receiver obtains the discrete-time samples.

Let $\bar{Y}_{n,m}$, $\bar{X}_{n,m}$, and $\bar{W}_{n,m}$ be the discrete-time received, target, and noise signals for the nth range bin during the mth PRI. Using these notations, we can rewrite the continuous-time input-output relationship in (24) as

$$\bar{Y}_{n,m} = \bar{X}_{n,m} + \bar{W}_{n,m}, \qquad (25)$$

where $\bar{W}_{n,m}$ follows the complex Gaussian with zero-mean and variance $B_\mathrm{s}N_0$, i.e., $\bar{W}_{n,m} \sim \mathcal{CN}(0, B_\mathrm{s}N_0)$ and $\bar{X}_{n,m}$ contains the target information for the relevant parameters $\{\tau_\ell, \nu_\ell, H_\ell\}_{\ell=1}^{L}$ as defined in (23). Suppose the ℓth target exists in the nth range bin, i.e., $\lfloor \tau_\ell / T_\mathrm{s} \rfloor = n$ for $n \in \{0, \ldots, N-1\}$. In this case, the target signal is defined as $\bar{X}_{n,m} = \sqrt{\beta_\ell} H_\ell e^{-j2\pi m \nu_\ell T_\mathrm{p}}$. Whereas, if a target is absent in the nth range bin, $\bar{X}_{n,m}$ is assumed to be null, i.e., $\bar{X}_{n,m} = 0$.

Using unit impulse function $\delta[n]$, we can define the discrete-time target signal $\bar{X}_{n,m}$ in compact form:

$$\bar{X}_{n,m} = \sum_{\ell=1}^{L} \sqrt{\beta_\ell} H_\ell \delta[n - U_\ell] e^{-j2\pi m \nu_\ell T_{\rm p}}, \quad (26)$$

where $U_\ell = \lfloor \tau_\ell / T_{\rm s} \rfloor \in \{0, \ldots, N-1\}$ is discrete random variable indicating the range information for the ℓth target.

Slow-time processing: In the pulse-Doppler radar system, the receiver also performs the matched filtering along the pulse dimension to increase the received power of the target signals. Recall that $0 \leq \nu_\ell T_{\rm p} \leq 1$ and the Doppler resolution is $1/MT_{\rm p}$. The limited Doppler resolution allows distinguishing target Doppler frequencies in the discrete set, i.e., $\nu_\ell T_{\rm p} \in \left\{0, \frac{1}{M}, \ldots, \frac{M-1}{M}\right\}$. With the discrete Doppler frequencies, the target signal in (26) boils down to

$$\bar{X}_{n,m} = \sum_{\ell=1}^{L} \sqrt{\beta_\ell} H_\ell \delta[n - U_\ell] e^{-j2\pi m \frac{V_\ell}{M}}, \quad (27)$$

where $V_\ell \in \{0, \ldots, M-1\}$ represents the Doppler bin index of the ℓth target. For given range bin index $n \in \{0, 1, \ldots, N-1\}$, the receiver takes an M-point discrete Fourier transform (DFT) operation as

$$\begin{aligned}\tilde{X}_{n,k} &= \frac{1}{\sqrt{M}} \sum_{m=0}^{M-1} \bar{X}_{n,m} e^{-j\frac{2\pi k}{M} m} \\ &= \sum_{\ell=1}^{L} \sqrt{\frac{\beta_\ell}{M}} H_\ell \delta[n - U_\ell] \sum_{m=0}^{M-1} e^{-jm\left(\frac{2\pi V_\ell}{M} - \frac{2\pi k}{M}\right)}. \end{aligned} \quad (28)$$

Using the fact that $\sum_{m=0}^{M-1} e^{-jm\left(\frac{2\pi V_\ell}{M} - \frac{2\pi k}{M}\right)} = M\delta[k - V_\ell]$, we can represent the (n,k) entry of the target signal as

$$\tilde{X}_{n,k} = \sum_{\ell=1}^{L} \sqrt{M\beta_\ell} H_\ell \delta[n - U_\ell] \delta[k - V_\ell]. \quad (29)$$

2) Discrete-time signal model: Let snr_n be the signal-to-noise ratio (SNR) of the nth range bin. From the radar equation in (3) and the target signal model in (29), the SNR under the target's presence in the nth range bin is defined as

$$\mathsf{snr}_n = \frac{M}{B_{\rm s} N_o} \frac{P_{\rm t} G_{\rm t} \sigma_{\rm rcs} A_{\rm eff}}{(4\pi)^2 \bar{d}_n^4}, \quad (30)$$

where $\bar{d}_n$ denotes the average distance from the nth range bin to the receiver, i.e., $\bar{d}_n = \frac{(2n+1)T_{\rm s} c}{4}$. Denoting $Y_{n,k} = \frac{1}{\sqrt{M}} \sum_{m=0}^{M-1} \bar{Y}_{n,m} e^{j\frac{2\pi mk}{M}}$ and $Z_{n,k} = \frac{1}{\sqrt{M}} \sum_{m=0}^{M-1} \bar{W}_{n,m} e^{j\frac{2\pi mk}{M}}$, the discrete-time input-output signal relationship for the (n,k) range-Doppler bin is given by

$$Y_{n,k} = \sqrt{\mathsf{snr}_n} X_{n,k} + Z_{n,k}, \quad (31)$$

where $Z_{n,k}$ is the normalized noise, which follows the complex Gaussian with zero-mean and unit variance, i.e., $Z_{n,k} \sim \mathcal{CN}(0,1)$, and $X_{n,k}$ is the target signal, which is defined as

$$X_{n,k} = \sum_{\ell=1}^{L} H_\ell \delta[n - U_\ell] \delta[k - V_\ell]. \quad (32)$$

APPENDIX II
PROOFS OF THEOREM

A. Proof of Lemma 1

To compute the MMSE estimator, we need to compute the expectation of $X_{n,k}$ given $Y_{n,k} = y_{n,k}$. This conditional expectation can be decomposed into as

$$\begin{aligned}&\mathbb{E}[X_{n,k}|Y_{n,k} = y_{n,k}] \\ &= \mathbb{E}[X_{n,k}|Y_{n,k} = y_{n,k}, X_{n,k} = 0]\mathbb{P}[X_{n,k} = 0|Y_{n,k} = y_{n,k}] \\ &\quad + \mathbb{E}[X_{n,k}|Y_{n,k} = y_{n,k}, X_{n,k} \neq 0]\mathbb{P}[X_{n,k} \neq 0|Y_{n,k} = y_{n,k}] \\ &= \mathbb{E}[X_{n,k}|Y_{n,k} = y_{n,k}, X_{n,k} \neq 0]\mathbb{P}[X_{n,k} \neq 0|Y_{n,k} = y_{n,k}],\end{aligned} \quad (33)$$

where the last equality follows from $\mathbb{E}[X_{n,k}|Y_{n,k} = y_{n,k}, X_{n,k} = 0] = 0$. To this end, we need to calculate both $\mathbb{E}[X_{n,k}|Y_{n,k} = y_{n,k}, X_{n,k} \neq 0]$ and $\mathbb{P}[X_{n,k} \neq 0|Y_{n,k} = y_{n,k}]$. In the case of $X_{n,k} \neq 0$, $Y_{n,k} = \sqrt{\mathsf{snr}_n} X_{n,k} + Z_{n,k}$ follows the complex Gaussian with mean $\sqrt{\mathsf{snr}_n}\mu_{\mathsf{T}}$ and variance $\mathsf{snr}_n \sigma_{\mathsf{T}}^2 + 1$, i.e., $\mathcal{CN}(\sqrt{\mathsf{snr}_n}\mu_{\mathsf{T}}, \mathsf{snr}_n \sigma_{\mathsf{T}}^2 + 1)$. In this case, the MMSE estimator is given by

$$\begin{aligned}&\mathbb{E}[X_{n,k}|Y_{n,k} = y_{n,k}, X_{n,k} \neq 0] \\ &\quad = \mu_{sfT} + \frac{\sqrt{\mathsf{snr}_n}\sigma_{\mathsf{T}}^2}{\mathsf{snr}_n \sigma_{\mathsf{T}}^2 + 1}(y_{n,k} - \sqrt{\mathsf{snr}_n}\mu_{\mathsf{T}}).\end{aligned} \quad (34)$$

From Baye's rule, we compute

$$\begin{aligned}&\mathbb{P}[X_{n,k} \neq 0|Y_{n,k} = y_{n,k}] \\ &= \frac{\mathbb{P}[X_{n,k} \neq 0|Y_{n,k} = y_{n,k}]\mathbb{P}(Y_{n,k} = y_{n,k})}{\mathbb{P}(Y_{n,k} = y_{n,k})} \\ &= \frac{\mathbb{P}(X_{n,k} \neq 0, Y_{n,k} = y_{n,k})}{\mathbb{P}(X_{n,k} = 0, Y_{n,k} = y_{n,k}) + \mathbb{P}(X_{n,k} \neq 0, Y_{n,k} = y_{n,k})}.\end{aligned} \quad (35)$$

The joint probabilities are computed as

$$\begin{aligned}&\mathbb{P}(X_{n,k} = 0, Y_{n,k} = y_{n,k}) \\ &\quad = \mathbb{P}(X_{n,k} = 0)\mathbb{P}(Y_{n,k} = y_{n,k}|X_{n,k} = 0) \\ &\quad = (1-\gamma)\frac{1}{\pi}e^{-|y_{n,k}|^2}\end{aligned} \quad (36)$$

and

$$\begin{aligned}&\mathbb{P}(X_{n,k} \neq 0, Y_{n,k} = y_{n,k}) \\ &\quad = \mathbb{P}(X_{n,k} \neq 0)\mathbb{P}(Y_{n,k} = y_{n,k}|X_{n,k} \neq 0) \\ &\quad = \gamma \times \frac{1}{\pi(\mathsf{snr}_n \sigma_{\mathsf{T}}^2 + 1)} e^{-\frac{|y_{n,k} - \sqrt{\mathsf{snr}_n}\mu_{\mathsf{T}}|^2}{\mathsf{snr}_n \sigma_{\mathsf{T}}^2 + 1}}.\end{aligned} \quad (37)$$

Invoking (36) and (37) into (35), we obtain the probability that the target is absent in the (n,k) range-Doppler bin as

$$\begin{aligned}&\mathbb{P}[X_{n,k} \neq 0|Y_{n,k} = y_{n,k}] \\ &= \frac{\gamma \frac{1}{\pi(\mathsf{snr}_n \sigma_{\mathsf{T}}^2 + 1)} e^{-\frac{|y_{n,k} - \sqrt{\mathsf{snr}_n}\mu_{\mathsf{T}}|^2}{\mathsf{snr}_n \sigma_{\mathsf{T}}^2 + 1}}}{(1-\gamma)\frac{1}{\pi}e^{-|y_{n,k}|^2} + \gamma \frac{1}{\pi(\mathsf{snr}_n \sigma_{\mathsf{T}}^2 + 1)} e^{-\frac{|y_{n,k} - \sqrt{\mathsf{snr}_n}\mu_{\mathsf{T}}|^2}{\mathsf{snr}_n \sigma_{\mathsf{T}}^2 + 1}}} \\ &= \frac{1}{1 + \frac{1-\gamma}{\gamma}(\mathsf{snr}_n \sigma_{\mathsf{T}}^2 + 1) e^{-|y_{n,k}|^2 + \frac{|y_{n,k} - \sqrt{\mathsf{snr}_n}\mu_{\mathsf{T}}|^2}{\mathsf{snr}_n \sigma_{\mathsf{T}}^2 + 1}}}.\end{aligned} \quad (38)$$

By plugging (34) and (38) into (33), we finally obtain the MMSE estimator as in (11). This completes the proof of lemma.

B. Proof of Theorem 2

We first define a binary random variable $U_{n,k} \in \{0,1\}$ with Bernoulli parameter γ to denote the target presence at the (n,k) range-Doppler bin. Similarly, we introduce the target complex amplitude parameter $A_{n,k}$, which is drawn from $\mathcal{CN}(\mu_{\mathsf{T}}, \sigma_{\mathsf{T}}^2)$. Then, our BG target signal $X_{n,k} \sim \mathsf{BG}(x|\mu_{\mathsf{T}}, \sigma_{\mathsf{T}}^2, \gamma)$ can be represented in a vector form $(U_{n,k}, A_{n,k})$. Using the chain rule, we decompose the mutual information as

$$\begin{aligned}
&I(X_{n,k};Y_{n,k}) \\
&\quad = I(U_{n,k}, A_{n,k}; Y_{n,k}) \\
&\quad = I(U_{n,k};Y_{n,k}) + I(A_{n,k};Y_{n,k}|U_{n,k}) \\
&\quad = I(U_{n,k};Y_{n,k}) + (1-\gamma) I(A_{n,k};Y_{n,k}|U_{n,k}=0) \\
&\qquad + \gamma I(A_{n,k};Y_{n,k}|U_{n,k}=1) \\
&\quad = I(U_{n,k};Y_{n,k}) + \gamma \log_2\left(1 + \mathsf{snr}_n \sigma_{\mathsf{T}}^2\right),
\end{aligned} \tag{39}$$

where the last equality comes from $I(A_{n,k};Y_{n,k}|U_{n,k}=0) = 0$.

We consider the NP detector to obtain the lower bound of $I(U_{n,k};Y_{n,k})$. Let $\hat{Y}_{n,k}$ be the output of the NP detector. Then, we can form the Markov chain $U_{n,k} \to Y_{n,k} \to \hat{Y}_{n,k}$. From the processing inequality, we have $I(U_{n,k};Y_{n,k}) \geq I(U_{n,k};\hat{Y}_{n,k})$. By noticing that $U_{n,k}$ and $\hat{Y}_{n,k}$ are the input and output of a binary asymmetric channel, we can lower bound the target detection information as

$$\begin{aligned}
I(U_{n,k};Y_{n,k}) &\geq I(U_{n,k};\hat{Y}_{n,k}) \\
&= \mathsf{H}_b((1-\gamma)P_{\mathsf{FA}} + \gamma(1-P_{\mathsf{MD}})) \\
&\quad - (1-\gamma)\mathsf{H}_b(P_{\mathsf{FA}}) - \gamma \mathsf{H}_b(P_{\mathsf{MD}}).
\end{aligned} \tag{40}$$

Plugging (40) into (39), we obtained the expression, which completes the proof.